



VOPO₄·2H₂O: Large-Scale Synthesis and Zinc-Ion Storage Application

Xianghua Zhang¹, Dan Yang¹, Weiling Liu² and Xianhong Rui^{1*}

¹ School of Materials and Energy, Guangdong University of Technology, Guangzhou, China, ² School of Materials Science and Engineering, Nanyang Technological University, Singapore, Singapore

OPEN ACCESS

Edited by:

Cheng Zhong,
Tianjin University, China

Reviewed by:

Lina Chen,
Harbin Institute of Technology,
Shenzhen, China

Hui Xia,
Nanjing University of Science
and Technology, China

*Correspondence:

Xianhong Rui
xhrui@gdut.edu.cn

Specialty section:

This article was submitted to
Electrochemical Energy Conversion
and Storage,
a section of the journal
Frontiers in Energy Research

Received: 28 June 2020

Accepted: 05 August 2020

Published: 04 September 2020

Citation:

Zhang X, Yang D, Liu W and Rui X
(2020) VOPO₄·2H₂O: Large-Scale
Synthesis and Zinc-Ion Storage
Application. *Front. Energy Res.* 8:211.
doi: 10.3389/fenrg.2020.00211

Rechargeable aqueous zinc ion batteries (ZIBs) have attracted increasingly solicitude in the application of large-scale electrochemical energy storage system (EES) as a result of their low-price, high security and environment-friendly. The synthesis of mass-produced electrode materials and the exploration of their potential electrochemical properties are essential steps to achieve superior large-scale EES. In this work, the large-scale preparation of vanadium oxyphosphate hydrate (VOPO₄·2H₂O) cathode material with impressively zinc storage ability is successfully demonstrated. Specially, it exhibits a high specific capacity of 165 mAh g⁻¹ at 0.05 A g⁻¹, and prominent rate property (90 and 75 mAh g⁻¹ at 2 and 5 A g⁻¹, respectively), as well as stable cyclability of 76% after 1000 cycles under a high current density of 5 A g⁻¹ within the voltage window of 0.4–1.6 V (versus Zn²⁺/Zn). Moreover, the VOPO₄·2H₂O not only spreads superiority in electrochemical performance, but also shows the advantages of scalable production based on simple controllable adjustment in synthesis, which is expected to exhibit great development potential in the field of large-scale EES application.

Keywords: zinc ion battery, cathode material, VOPO₄·2H₂O, large-scale synthesis, long cycling performance

INTRODUCTION

With the aggravation of the serious energy crisis, it is particularly important to maximize energy utilization through energy storage and conversion technologies (Palanisamy et al., 2016; Guo Q. et al., 2020; Yang et al., 2020; Zhang S. et al., 2020). Rechargeable batteries recently have received tremendous solicitude as a result of their broad prospect and great potential in energy storage application such as portable electronic device, electric vehicles, and large-scale grid (Xia et al., 2018; Ao et al., 2019; Xiong et al., 2020). Due to the extremely finite resources and steeply rising prices of lithium and its increasingly concerned safety issues, lithium-ion batteries (LIBs) barely meet the growing energy demand and seriously hinder their further growing for large-scale electrochemical energy storage (EES) in the modern society (Chen L. et al., 2019; Lin et al., 2019; Li C. et al., 2020; Wang et al., 2020).

While, aqueous rechargeable alkaline metal ion batteries based on environmentally friendly water electrolytes give prominence to the merits of low price, good safety and high ion conductivity (two orders of magnitude higher than that of traditional non-aqueous rechargeable batteries), which in turn become the most promising alternatives to traditional LIBs in large-scale EES (Chen D. et al., 2019; Li G. et al., 2020). Among these rising aqueous rechargeable batteries, aqueous zinc ion batteries (ZIBs) are characterized as the potential representative owing to the low redox potential (−0.76 V vs. SHE.), high theoretical specific capacities

(819 mAh g⁻¹ and 5845 mAh cm⁻³), rich reserves (as the fourth “common” metal in the crust of earth), low cost and outstanding water compatibility of the zinc metal (Xia et al., 2017; Song et al., 2018; Li et al., 2019). However, the current available cathode materials of ZIBs deliver unsatisfactory performance [e.g., the low discharge capacity of Prussian blue analogs (Ke et al., 2017), the poor cycling stability of MnO₂ polymorphs (Sun et al., 2017), etc.], seriously restricting the development and commercialization of aqueous ZIBs. Recently, vanadium-based electrode materials show impressive electrochemical properties in alkaline metal ion batteries because of their multiple valence changes and high electrochemical activity in chemical energy storage (Deng et al., 2020; Xie et al., 2020; Zhang X. et al., 2020). Among various vanadium-based electrode materials (Yue et al., 2016; Guo X. et al., 2020; Liu et al., 2020), layered VOPO₄·2H₂O has been widely concerned. This electrode material provides adjustable layer spacing to accommodate the intercalated zinc ions, and with the help of water, the zinc ions are more easily intercalated into the VOPO₄·2H₂O material (Huang et al., 2014; Peng et al., 2017; Tang et al., 2020). Additionally, the VOPO₄·2H₂O material can also store electric charge during anionic redox reaction process (Yang et al., 2020). There are many recent reports about VOPO₄·2H₂O electrode material applied in aqueous ZIBs, but it is invariably found that the prepared VOPO₄·2H₂O material showed low output in production and unsatisfactory performance in zinc storage property, which is in a difficult position to meet the demand of large-scale EES application. For instance, Shi et al. studied the zinc storage performance of the VOPO₄·2H₂O cathode synthesized by a reflux method. And it is shown that the VOPO₄·2H₂O cathode only released 60 mAh g⁻¹ at a high electric current density of 5 A g⁻¹ and an unobtrusive cycle-life with only 500 cycles at 2 A g⁻¹ (Shi et al., 2019). Consequently, it is essential to produce a high performance VOPO₄·2H₂O cathode material with large-scale production.

Herein, a facile route has been designed for the large-scale synthesis of VOPO₄·2H₂O sample by a simple solid-state method, which is in great favor of extending the application of aqueous ZIBs in large-scale storage devices. The VOPO₄·2H₂O electrode delivers an excellent zinc storage ability with high reversible discharge specific capacity (165 mAh g⁻¹ at 0.05 A g⁻¹) and good rate characteristics (90 and 75 mAh g⁻¹ at 2 and 5 A g⁻¹, respectively) in the voltage window of 0.4–1.6 V (versus Zn²⁺/Zn). Moreover, the VOPO₄·2H₂O electrode exhibits a superior long cycle performance with stable Coulombic efficiency evolution during the repetitive electrochemical process (i.e., 76% capacity retention up to the 1000th cycle at a high electric current density of 5 A g⁻¹).

MATERIALS AND METHODS

Synthesis of VOPO₄·2H₂O Sample

In a typical procedure, a suspension consisting of 1440 mL deionized water (DI H₂O), 60 g vanadium pentoxide (V₂O₅) powders, and 360 mL concentrated phosphoric acid (85% H₃PO₄) was transferred to an agate tank and ball-milled at an

appropriate speed of 500 rpm min⁻¹ for 30 h. After the program completed, the yellow-greenish products were centrifuged and washed by water and acetone several times. Conclusively, the resulting product was dried in a vacuum (60°C for 8 h) to yield VOPO₄·2H₂O sample. Here, it is noteworthy that the total mass of the as-obtained VOPO₄·2H₂O powder prepared by this simple method can reach to a mass production of ~80 g, which is nearly 100 times of the yield via the traditional reflux method (Shi et al., 2019).

Characterization

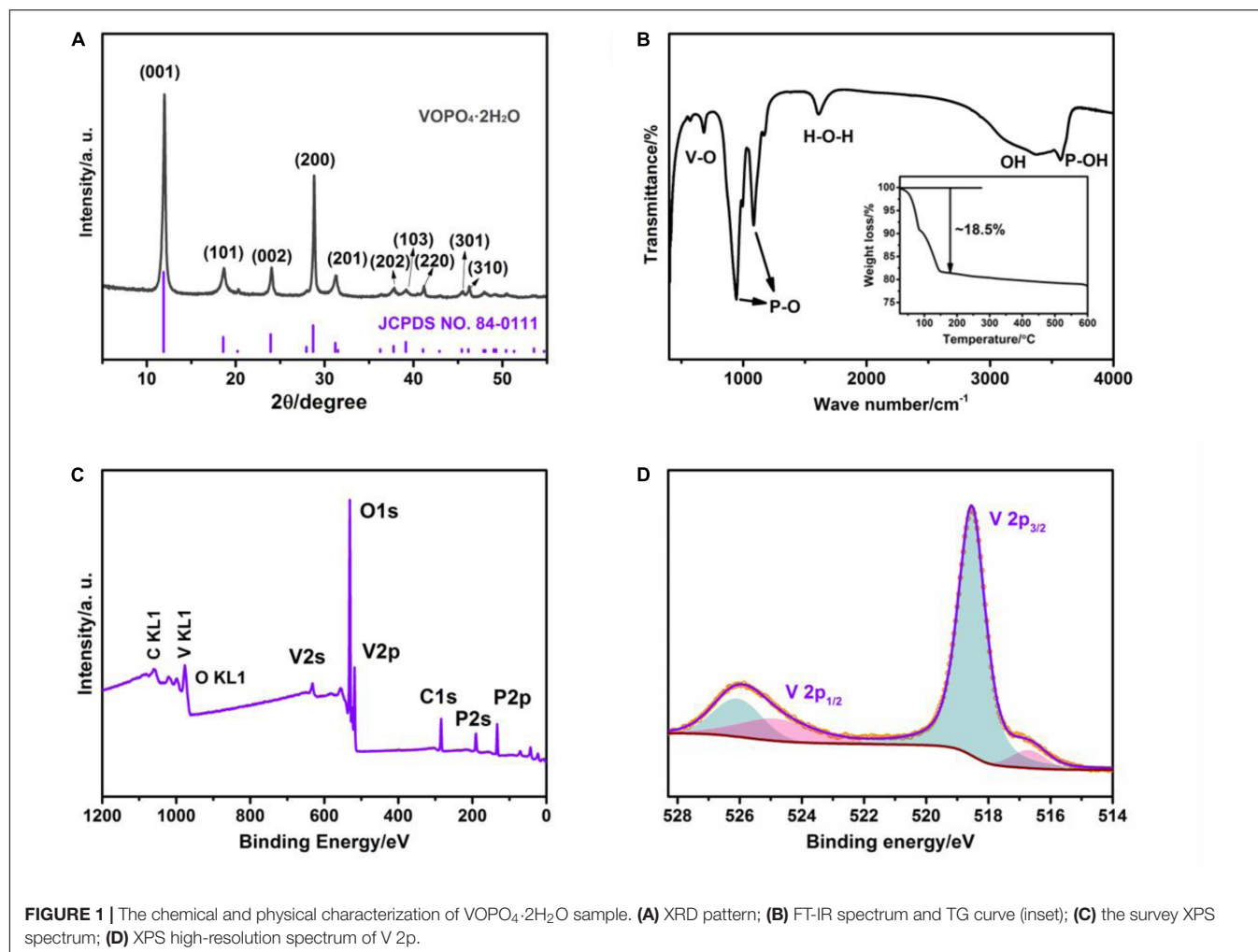
The polycrystalline X-ray diffraction (XRD, Rigaku SmartLab) with Cu K α X-ray source ($\lambda = 0.154056$ nm) was employed to accurately determine the crystallographic structure of the prepared sample. The fourier transform infrared spectroscopy (FTIR, Nicolet 6700) was detected within a wavenumber interval of 4000–500 cm⁻¹. The TG curve was obtained by a thermal gravimetric analysis (TGA/DSC3 +) instrument from 25 to 600°C in air atmosphere (heating rate: 10°C min⁻¹). The X-ray photoelectron spectroscopy (XPS, Escalab 250Xi) was used to analysis phase composition and chemical state of element for the final product. The field-emission scanning electron microscopy (FESEM, Hitach SU-8220) and transmission electron microscopy (TEM, JEM-2100F) instrument were used to measure the morphology for the synthesized sample.

Electrochemical Measurement

The working electrode (i.e., cathode) contained 60 wt% active material VOPO₄·2H₂O, 30 wt% conductive carbon nanotubes and 10 wt% binder polyvinylidene fluoride in N-methyl pyrrolidone solvent. After thorough stirring, the homogenous slurry was coated on titanium foils and dried in a vacuum oven at 60°C for a whole night. The CR2032-type coin cells were used to assemble button cells, including the above working cathode, the metallic zinc anode and 3 M Zn (CF₃SO₃)₂ electrolyte as well as glass-fiber separator in air atmosphere. Galvanostatic charge–discharge cycling and rate performance tests were investigated within the voltage test window of 0.4–1.6 V (vs Zn²⁺/Zn) by using NEWARE system. Electrochemical impedance spectroscopy (EIS) studies were executed with the button cell on an electrochemical workstation (Multi-Autolab M204) within the frequency domain of 10⁵–10⁻² Hz. Cyclic voltammetry (CV) were also tested by the Multi-Autolab M204 measurement at different potential scan rates scanning from 0.1 to 0.5 mV s⁻¹. It is mentioned here that, before electrochemical testing, the VOPO₄·2H₂O cathode was initially activated by discharging to 0.4 V.

RESULTS AND DISCUSSION

The crystallographic structure and phase purity of the resultant product is measured by XRD technique. As shown in **Figure 1A**, all observed reflections completely matched with the standard pattern of the tetragonal VOPO₄·2H₂O (space group: P4/n, JCPDS card: 84-0111). And no detectable impurity peaks can be found, indicating the high purity of VOPO₄·2H₂O crystal (Zhou



et al., 2016). The FT-IR analysis is carried out to confirm the existence of various groups in the $\text{VOPO}_4 \cdot 2\text{H}_2\text{O}$ sample, and its spectrum is exhibited in **Figure 1B**. The absorption peaks located at about 684 cm^{-1} is attributed to the V-O extension vibration. The peaks at 950 and 1080 cm^{-1} can be related to the P-O stretching vibration in PO_4 group (Bao et al., 2011). The absorption peaks of P-OH and O-H stretching vibration in H_2O are observed at 3600 and 3400 cm^{-1} , respectively. The peak at 1616 cm^{-1} corresponds to the H-O-H bending vibration of interlayer H_2O (Zhou et al., 2014). These characteristic peaks are proved to be in agreement with the chemical composition of $\text{VOPO}_4 \cdot 2\text{H}_2\text{O}$ (Patel et al., 2003). Additionally, the water content of the final product is confirmed by the TG analysis in the air test environment within the operating temperature window of 25 – 600°C . As shown in the illustration of **Figure 1B**, the weight loss percentage of the final product between 25 and 150°C is calculated to be 18.5% , which conforming with the evaporation loss of two crystal water molecules in per mole of as-obtained sample (Zhou et al., 2018; Hyoungh et al., 2019). The surface element analysis and chemical states for as-prepared composite were further identified via XPS spectra. As demonstrated in **Figure 1C**, P, O, and V elements were presented

in $\text{VOPO}_4 \cdot 2\text{H}_2\text{O}$ survey spectrum, and the high-resolution XPS spectra of P2p and O1s are displayed in **Supplementary Figure 1 (Supplementary Material)**, which are in good accordance with the reported result in the recent literature (Verma et al., 2019). According to the high-resolution V2p XPS spectrum in **Figure 1D**, it is clearly observed two sharp peaks located at the binding energy of 518.5 and 516.6 eV , according with $\text{V}2\text{p}_{3/2}$ of V^{5+} and V^{4+} , respectively. And the other peaks at 525.8 and 524.6 eV are associated with $\text{V}2\text{p}_{1/2}$ of V^{5+} and V^{4+} , respectively (Chen et al., 2018).

The morphology and detailed structure of $\text{VOPO}_4 \cdot 2\text{H}_2\text{O}$ sample are investigated by FESEM and TEM analysis. The $\text{VOPO}_4 \cdot 2\text{H}_2\text{O}$ sample displays irregular bulk morphology with the size of 0.5 – $2 \mu\text{m}$ from the SEM images (**Figures 2a,b**). The TEM images in **Figures 2c,d** indicate that this bulk material contains many nanosheets. Moreover, a lattice fringe with the d-spacing of $\approx 0.36 \text{ nm}$ can be also investigated in the HRTEM image (**Figure 2e**), corresponding to the (002) crystal plane of the tetragonal $\text{VOPO}_4 \cdot 2\text{H}_2\text{O}$.

In order to systematically investigate the zinc storage performance of $\text{VOPO}_4 \cdot 2\text{H}_2\text{O}$ cathode in large-scale EES applications, a series of electrochemical tests based on coin

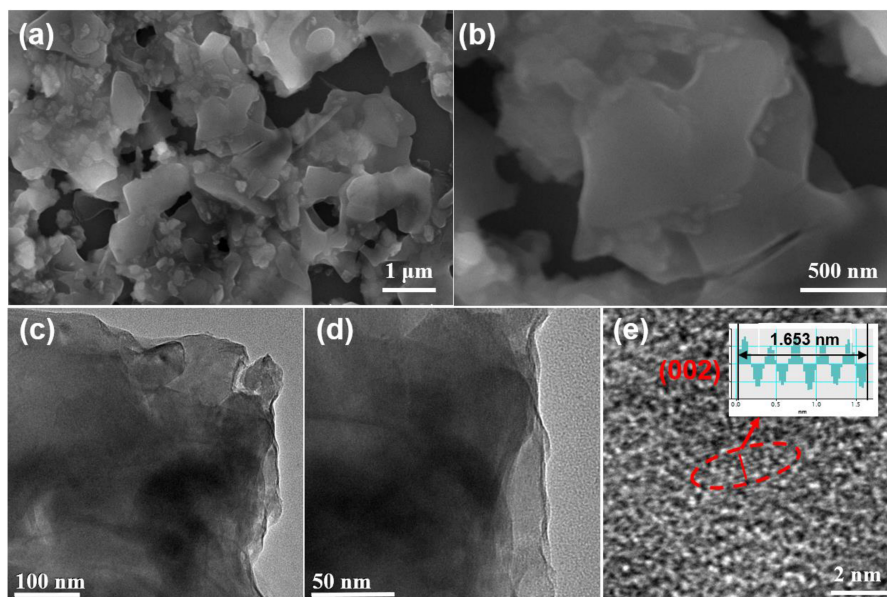


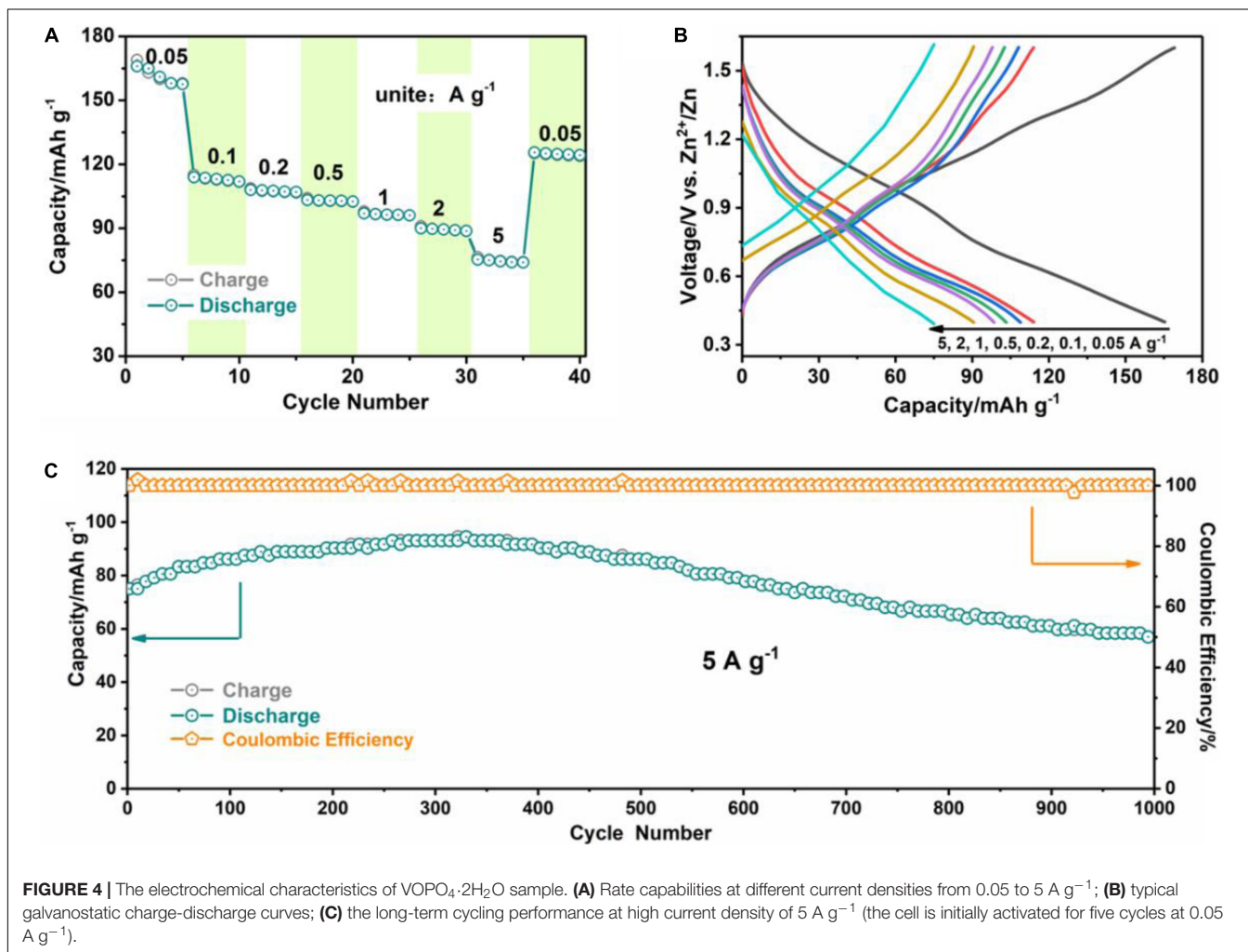
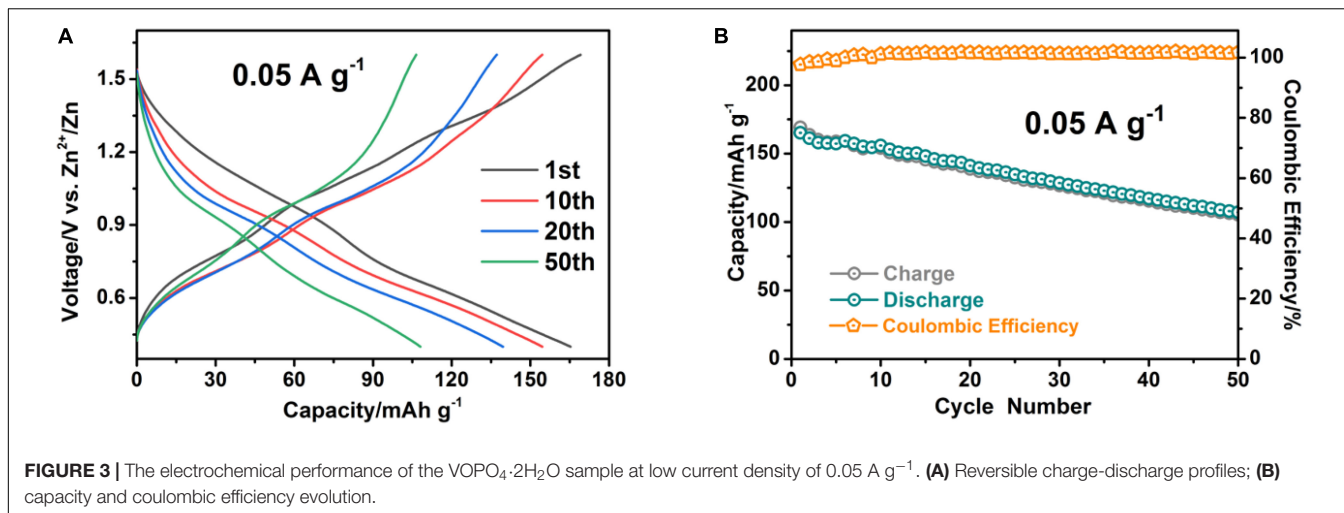
FIGURE 2 | The microstructure and morphology of the $\text{VOPO}_4 \cdot 2\text{H}_2\text{O}$ sample. **(a,b)** SEM images under different scanning resolutions; **(c,d)** TEM images; **(e)** HRTEM image.

cells employing 3 M $\text{Zn}(\text{CF}_3\text{SO}_3)_2$ aqueous electrolyte are carried out within the voltage window of 0.4–1.6 V (versus Zn^{2+}/Zn). The typical galvanostatic charge-discharge profiles from the 1st to 50th cycles are revealed in **Figure 3A**. Two stable flat charge voltages at 0.7 and 1 V appeared under the driven forward by zinc ions over cycles (Shi et al., 2019). The associated differential capacity curves are also displayed in **Supplementary Figure 2**, Supporting information. And two apparent redox peaks of 0.58/0.76 and 0.92/1.05 V are associated with the two-step Zn^{2+} (de)intercalation processes. Moreover, the representative cyclic voltammetry test of the $\text{VOPO}_4 \cdot 2\text{H}_2\text{O}$ electrode at 0.1 mV s^{-1} scan rate in the voltage range of 0.4–1.6 V (vs Zn^{2+}/Zn) is presented in **Supplementary Figure 3**, Supporting information. The two apparent redox peaks are clearly observed in the CV curves, which are almost identical to the result obtained from the associated differential capacity curves. **Figure 3B** exhibits the capacity and coulombic efficiency of $\text{VOPO}_4 \cdot 2\text{H}_2\text{O}$ cathode at 0.05 A g^{-1} in the voltage range of 0.4–1.6 V versus Zn^{2+}/Zn . Obviously, the $\text{VOPO}_4 \cdot 2\text{H}_2\text{O}$ cathode exhibited a disappointing cycling stability at the low electric current density of 0.05 A g^{-1} , this is mainly due to the presence or co-intercalation of water in the active material and the side reaction of the electrolyte caused during the longer Zn^{2+} insertion process at the low current density, the zinc storage capacity of $\text{VOPO}_4 \cdot 2\text{H}_2\text{O}$ electrode is on the decline in the previous activation stages, leading to the discharge specific capacity of the $\text{VOPO}_4 \cdot 2\text{H}_2\text{O}$ cathode decayed from 165 to 108 mAh g^{-1} over 50 cycles.

Additionally, the rate performance and its associated voltage profiles of the $\text{VOPO}_4 \cdot 2\text{H}_2\text{O}$ electrode under various current densities are exhibited in **Figures 4A,B**. The $\text{VOPO}_4 \cdot 2\text{H}_2\text{O}$ electrode displays high reversible specific capacities of 165, 114,

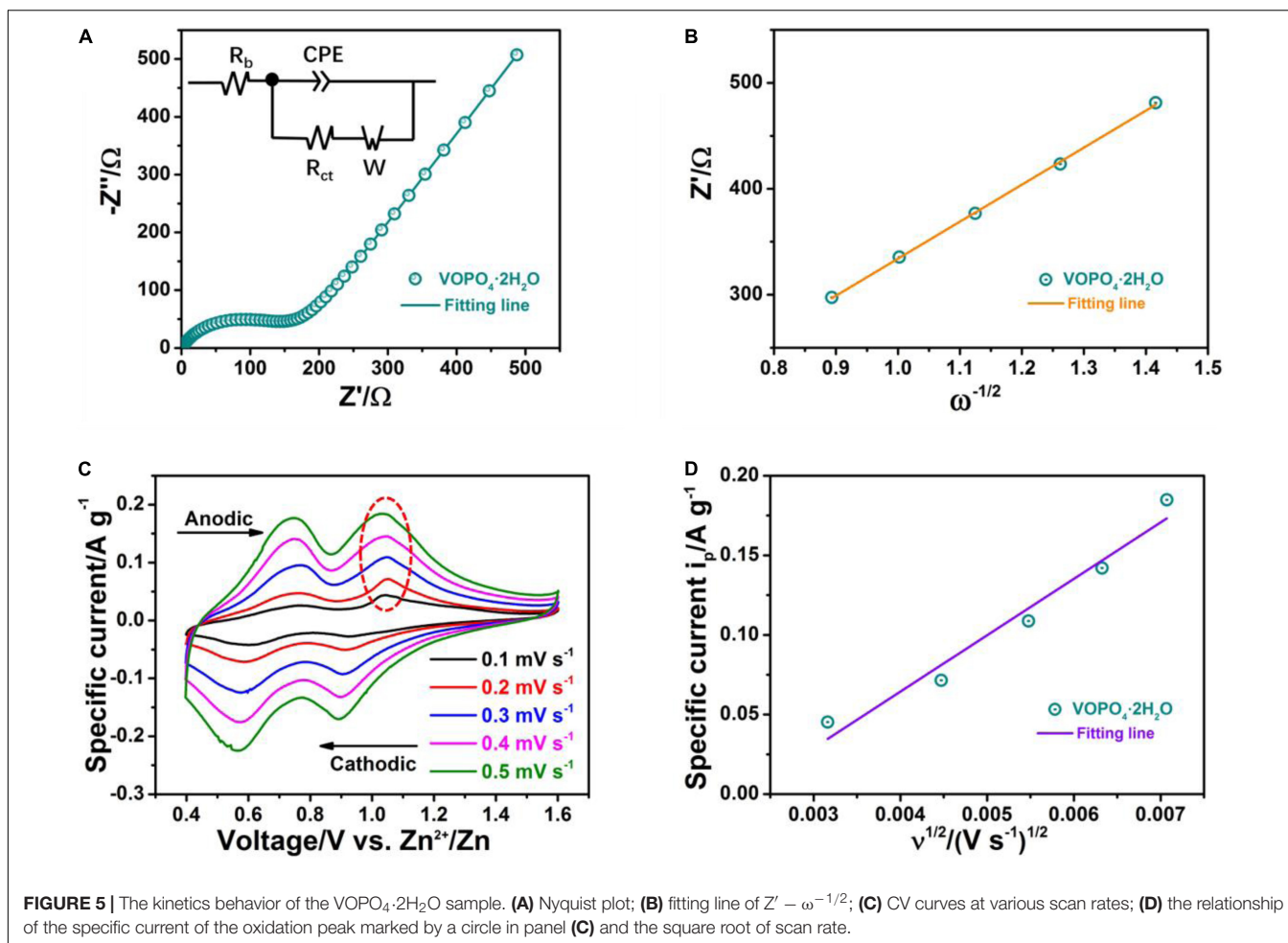
108, 103, 97, and 90 mAh g^{-1} (according to the discharge specific capacities at 1st, 6th, 11th, 16th, 21th, and 26th cycles) at 0.05, 0.1, 0.2, 0.5, 1, and 2 A g^{-1} , respectively. Even at a high electric current density of 5 A g^{-1} , the $\text{VOPO}_4 \cdot 2\text{H}_2\text{O}$ cathode can still achieve an attractive reversible capacity of 75 mAh g^{-1} . And a reversible specific capacity of 125 mAh g^{-1} remains when the electric current density is changed back to 0.05 A g^{-1} , manifesting the reversible redox kinetic of $\text{VOPO}_4 \cdot 2\text{H}_2\text{O}$ electrode. Furthermore, the cycling behavior of the $\text{VOPO}_4 \cdot 2\text{H}_2\text{O}$ electrode has been examined at the high electric current density of 5 A g^{-1} displayed in **Figure 4C** and **Supplementary Figure 4**, Supporting information. The $\text{VOPO}_4 \cdot 2\text{H}_2\text{O}$ electrode not only holds the general shape of the galvanostatic charge-discharge profiles during the long term cycle (1000 times) at 5 A g^{-1} , but also retains a stable reversible specific capacity of 57 mAh g^{-1} with 76% of capacity retention after 1000 cycles, which is exceptional to that of recently covered $\text{VOPO}_4 \cdot 2\text{H}_2\text{O}$ based aqueous ZIBs (Shi et al., 2019).

Furthermore, EIS analysis is also measured to explore the electrochemical kinetics of $\text{VOPO}_4 \cdot 2\text{H}_2\text{O}$ cathode for zinc storage behavior. As shown in **Figure 5A**, the Nyquist plot of the $\text{VOPO}_4 \cdot 2\text{H}_2\text{O}$ electrode is evaluated at the 3rd fully charged state. It includes the semicircle part of high-middle frequency range and the slant part of low frequency, which represent charge transfer impedance (R_{ct}) between the $\text{VOPO}_4 \cdot 2\text{H}_2\text{O}$ electrode and electrolyte and Warburg resistance (W) corresponded to the zinc ion diffusion in active material, respectively. Equivalent circuit model is established by EIS analysis and shown in the inset of **Figure 5A**. It has been calculated that the R_{ct} -value of $\text{VOPO}_4 \cdot 2\text{H}_2\text{O}$ electrode is simulated to be around 184 Ω , smaller than that of recent reported $\text{VOPO}_4 \cdot 2\text{H}_2\text{O}$ electrodes in aqueous ZIBs (Shi et al., 2019). It is remarkable that the



smaller R_{ct} -value indicates the more relax desolvation at the interphase and faster zinc ions diffusion. Here, the apparent diffusion coefficient of Zn²⁺ ($D_{Zn^{2+}}$) for the VOPO₄·2H₂O electrode is explored and calculated by applying the Equation:

$D_{Zn^{2+}} = 0.5R^2T^2/S^2n^4F^4C^2\sigma^2$ (Yang et al., 2019). In the formula, R , T , and F stand for the universal gas constant, absolute temperature and the Faraday constant, corresponding to the related values of 8.314 J mol⁻¹ K⁻¹, 298.15 K, and



96,485 C mol⁻¹, respectively. S , n , and C are delegated the active surface area of the cathode, the number of electrons migration and the concentration of zinc ions, respectively. The Warburg coefficient σ is related to the gradient of the fitting linear of $Z' - \omega^{-1/2}$ based on the standard equation: $Z' = R + \sigma\omega^{-1/2}$ (Chen S. et al., 2019). Where ω astricts the low frequency area, R is a frequency independent kinetic parameter, whose value is approximately equal to that of R_{ct} in the Nyquist plot. **Figure 5B** displays the linear fitting of $Z' - \omega^{-1/2}$ and shows a faster diffusion process (3.2×10^{-14} cm² s⁻¹) of zinc ions during the repeated charge/discharge process. Overall, such small charge transfer impedance and large apparent diffusion coefficient are favorable to promote the (de)intercalation of zinc ions, exhibiting outstanding large current performance and excellent rate capability. The cyclic voltammety (CV) technique was performed to further understand the zinc storage performance of the as-obtained VOPO₄·2H₂O cathode. The CV profiles at different potential scanning rates ranging from 0.1 to 0.5 mV s⁻¹ are revealed in **Figure 5C**, two well-defined sharp redox reaction peaks are observed, corresponding to the two-step Zn²⁺ (de)intercalation behavior, which also are well consisted with the voltage platforms appeared in galvanostatic charge-discharge curves. What's more, the sharp

defined redox peaks could still be kept at the high scanning rate of 0.5 mV s⁻¹, although the redox peaks increased in width and height with the increment of the scan rate, suggesting the good reaction kinetics and excellent rate performance of VOPO₄·2H₂O cathode. Furthermore, the zinc ion diffusion coefficient $D_{Zn^{2+}}$ can be also obtained base on the data from the CV profiles and applying of the Randles-Sevcik equation (Wei et al., 2017):

$$i_p = (2.65 \times 10^5) n^{3/2} S D_{Zn^{2+}}^{1/2} C v^{1/2}$$

wherein i_p is the specific peak current, n stands for the number of electrons migration, S is the actual contact area between the cathode active material and electrolyte, C is referred to the concentration of Zn²⁺, and v is scanning rate. $D_{Zn^{2+}}$ is estimated from the slope of fitting linear of the specific current i_p along with the square root of the scan rate $v^{1/2}$. Based on the slope value of $i_p - v^{1/2}$ in **Figure 5D**, the zinc ion diffusion coefficient ($D_{Zn^{2+}}$) of VOPO₄·2H₂O cathode is calculated to be $\sim 2.0 \times 10^{-13}$ cm² s⁻¹, according well with the value of Zn²⁺ coefficient obtained from EIS measurement. And the fast charge transfer kinetics of Zn²⁺ (de)intercalation for the VOPO₄·2H₂O cathode is further highlighted via the applying of CV technique.

CONCLUSION

In this study, we have developed a facial solid state reaction to prepare the $\text{VOPO}_4 \cdot 2\text{H}_2\text{O}$ sample with industrial mass production grade. When the $\text{VOPO}_4 \cdot 2\text{H}_2\text{O}$ is applied as cathode material of rechargeable aqueous ZIBs, it displays high reversible specific capacity (165 mAh g^{-1} at 0.05 A g^{-1} within the voltage window of $0.4\text{--}1.6 \text{ V}$ (vs. Zn^{2+}/Zn) and superior rate capability (90 and 75 mAh g^{-1} at 2 and 5 A g^{-1} , respectively), as well as outstanding stable cyclicality (76% of capacity retention after 1000 cycles at 5 A g^{-1}). In addition to the excellent zinc storage performance, the $\text{VOPO}_4 \cdot 2\text{H}_2\text{O}$ cathode can easily achieve mass production based on simple effective regulation and control in synthesis, showing great development potential in the field of large-scale EES.

DATA AVAILABILITY STATEMENT

The raw data supporting the conclusions of this article will be made available by the authors, without undue reservation.

REFERENCES

- Ao, H., Zhao, Y., Zhou, J., Cai, W., Zhang, X., Zhu, Y., et al. (2019). rechargeable aqueous hybrid ion batteries: developments and prospects. *J. Mater. Chem. A* 7, 18708–18734. doi: 10.1039/C9TA06433H
- Bao, C., Guo, Y., Song, L., Lu, H., Yuan, B., and Hu, Y. (2011). Facile Synthesis of Poly(vinyl alcohol)/alpha-Titanium phosphate nanocomposite with markedly enhanced properties. *Ind. Eng. Chem. Res.* 50, 11109–11116. doi: 10.1021/ie200700t
- Chen, D., Rui, X., Zhang, Q., Geng, H., Gan, L., Zhang, W., et al. (2019). Persistent Zinc-ion storage in mass-produced V_2O_5 architecture. *Nano Energy* 60, 171–178. doi: 10.1016/j.nanoen.2019.03.034
- Chen, L., Chen, L., Zhai, W., Li, D., Lin, Y., Guo, S., et al. (2019). Tunable synthesis of Li_xMnO_2 nanowires for aqueous li-ion hybrid supercapacitor with high rate capability and ultra-long cycle life. *J. Power Sources* 413, 302–309. doi: 10.1016/j.jpowsour.2018.12.026
- Chen, S., Zhang, Y., Geng, H., Yang, Y., Rui, X., and Li, C. (2019). Zinc ions pillared vanadate cathodes by chemical pre-intercalation towards long cycling life and low-temperature zinc ion batteries. *J. Power Sources* 441, 227192. doi: 10.1016/j.jpowsour.2019.227192
- Chen, N., Zhou, J., Zhu, G., Kang, Q., Ji, H., Zhang, Y., et al. (2018). A High-performance asymmetric supercapacitor based on vanadyl phosphate/carbon nanocomposites and polypyrrole-derived carbon nanowires. *Nanoscale* 10, 3709–3719. doi: 10.1039/C7NR08909K
- Deng, C., Xie, X., Han, J., Tang, Y., Gao, J., Liu, C., et al. (2020). A sieve-functional and uniform-porous kaolin layer toward stable zinc metal anode. *Adv. Funct. Mater.* 30:2000599. doi: 10.1002/adfm.202000599
- Guo, Q., Li, S., Liu, X., Lu, H., Chang, X., Zhang, H., et al. (2020). Ultrastable sodium-sulfur batteries without polysulfides formation using slit ultramicropore carbon carrier. *Adv. Sci.* 7:1903246. doi: 10.1002/advs.201903246
- Guo, X., Zhou, J., Bai, C., Li, X., Fang, G., and Liang, S. (2020). Zn/MnO₂ battery chemistry with dissolution-deposition mechanism. *Mater. Today Energy* 16:100396. doi: 10.1016/j.mtener.2020.100396
- Huang, H.-L., Lii, K.-H., and Wang, S.-L. (2014). Really understanding layered vanadyl phosphate hydrates. *J. Chin. Chem. Soc.* 61, 199–206. doi: 10.1002/jccs.201300520
- Hyoung, J., Heo, J. W., Chae, M. S., and Hong, S.-T. (2019). Electrochemical exchange reaction mechanism and the role of additive water to stabilize the structure of VOPO_4 center dot $2\text{H}_2\text{O}$ as a cathode material for potassium-ion batteries. *ChemSuschem* 12, 1069–1075. doi: 10.1002/cssc.201802527

AUTHOR CONTRIBUTIONS

XR directed the project. XZ, DY, and WL performed the experiment, analyzed data, and wrote the manuscript. All authors contributed to the discussion.

FUNDING

The authors gratefully acknowledge the National Natural Science Foundation of China (Grant Nos. 51972067 and 51802044) and Guangdong Natural Science Funds for Distinguished Young Scholar (Grant No. 2019B151502039).

SUPPLEMENTARY MATERIAL

The Supplementary Material for this article can be found online at: <https://www.frontiersin.org/articles/10.3389/fenrg.2020.00211/full#supplementary-material>

- Ke, L., Song, B., Zhang, Y., Ma, H., and Zhang, J. (2017). Encapsulation of zinc hexacyanoferrate nanocubes with manganese oxide nanosheets for high-performance rechargeable zinc-ion batteries. *J. Mater. Chem. A* 5, 23628–23633. doi: 10.1039/C7TA07834J
- Li, C., Wang, B., Chen, D., Gan, L., Feng, Y., Zhang, Y., et al. (2020). Topotactic transformation synthesis of 2D Ultrathin GeS_2 nanosheets toward high-rate and high-energy-density sodium-Ion Half/Full Batteries. *ACS Nano* 14, 531–540. doi: 10.1021/acsnano.9b06855
- Li, G., Chen, W., Zhang, H., Gong, Y., Shi, F., Wang, J., et al. (2020). Membrane-Free Zn/MnO₂ flow battery for large-scale energy storage. *Adv. Energy Mater.* 10:1902085. doi: 10.1002/aenm.201902085
- Li, X., Tang, Y., Lv, H., Wang, W., Mo, F., Liang, G., et al. (2019). Recent advances in flexible aqueous zinc-based rechargeable batteries. *Nanoscale* 11, 17992–18008. doi: 10.1039/C9NR06721C
- Lin, B., Zhu, X., Fang, L., Liu, X., Li, S., Zhai, T., et al. (2019). Birnessite Nanosheet Arrays with High K Content as a High-Capacity and Ultrastable Cathode for K-Ion Batteries. *Adv. Mater.* 31:e1900060. doi: 10.1002/adma.201900060
- Liu, S., Zhu, H., Zhang, B., Li, G., Zhu, H., Ren, Y., et al. (2020). Tuning the kinetics of zinc-ion insertion/extraction in V_2O_5 by in situ polyaniline intercalation enables improved aqueous zinc-ion storage performance. *Adv. Mater.* 32:2001113. doi: 10.1002/adma.202001113
- Palanisamy, K., Um, J. H., Jeong, M., and Yoon, W.-S. (2016). Porous $\text{V}_2\text{O}_5/\text{RGO}/\text{CNT}$ hierarchical architecture as a cathode material: emphasis on the contribution of surface lithium storage. *Sci. Rep. U. K.* 6:31275. doi: 10.1038/srep31275
- Patel, V., Chudasam, A., Nivsarkar, M., Vasu, K., and Shishoo, C. (2003). Synthesis and Characterization of an VOPO_4 -polyaniline lamellar hybrid compound. *Solid State Sci.* 5, 611–613. doi: 10.1016/S1293-2558(03)00046-3
- Peng, L., Zhu, Y., Peng, X., Fang, Z., Chu, W., Wang, Y., et al. (2017). effective interlayer engineering of two-dimensional VOPO_4 nanosheets via controlled organic intercalation for improving alkali ion storage. *Nano Lett.* 17, 6273–6279. doi: 10.1021/acs.nanolett.7b02958
- Shi, H., Song, Y., Qin, Z., Li, C., and Sun, X. (2019). Inhibiting $\text{VOPO}_4 \cdot 2\text{H}_2\text{O}$ decomposition and dissolution in rechargeable aqueous zinc batteries to promote voltage and capacity stabilities. *Angew. Chem.* 58, 16057–16061. doi: 10.1002/anie.201908853
- Song, M., Tan, H., Chao, D., and Fan, H. J. (2018). Recent advances in Zn-Ion batteries. *Adv. Funct. Mater.* 28:1802564. doi: 10.1002/adfm.201802564
- Sun, W., Wang, F., Hou, S., Yang, C., Fan, X., Ma, Z., et al. (2017). Zn/MnO₂ battery chemistry With H^+ and Zn^{2+} coinsertion. *J. Am. Chem. Soc.* 139, 9775–9778. doi: 10.1021/jacs.7b04471

- Tang, Y., Liu, C., Zhu, H., Xie, X., Gao, J., Deng, C., et al. (2020). Ion-confinement effect enabled by gel electrolyte for highly reversible dendrite-free zinc metal anode. *Energy Storage Mater.* 27, 109–116. doi: 10.1016/j.ensm.2020.01.023
- Verma, V., Kumar, S., Manalastas, W. Jr., Zhao, J., Chua, R., Meng, S., et al. (2019). Layered VOPO₄ as a cathode material for rechargeable zinc-ion battery: effect of polypyrrole intercalation in the host and water concentration in the electrolyte. *ACS Appl. Energy Mater.* 2, 8667–8674. doi: 10.1021/acsam.9b01632
- Wang, B., Ang, E. H., Yang, Y., Zhang, Y., Geng, H., Ye, M., et al. (2020). Interlayer engineering of molybdenum trioxide toward high-capacity and stable sodium ion Half/Full batteries. *Adv. Funct. Mater.* 30:2001708. doi: 10.1002/adfm.202001708
- Wei, T., Yang, G., and Wang, C. (2017). Bottom-up assembly of strongly-coupled Na₃V₂(PO₄)₃/C into hierarchically porous hollow nanospheres for high-rate and -stable Na-ion Storage. *Nano Energy* 39, 363–370. doi: 10.1016/j.nanoen.2017.07.019
- Xia, C., Guo, J., Lei, Y., Liang, H., and Alshareef, H. N. (2017). Rechargeable aqueous zinc-ion battery based on porous framework zinc pyrovanadate intercalation cathode. *Adv. Mater.* 30:1705580. doi: 10.1002/adma.201705580
- Xia, H., Zhu, X., Liu, J., Liu, Q., Lan, S., Zhang, Q., et al. (2018). A monoclinic polymorph of sodium birnessite for ultrafast and ultrastable sodium ion storage. *Nat. Commun.* 9:5100. doi: 10.1038/s41467-018-07595-y
- Xie, X., Liang, S., Gao, J., Guo, S., Guo, J., Wang, C., et al. (2020). Manipulating the ion-transfer kinetics and interface stability for high-performance zinc metal anodes. *Energy. Environ. Sci.* 13, 503–510. doi: 10.1039/c9ee03545a
- Xiong, P., Zhang, F., Zhang, X., Wang, S., Liu, H., Sun, B., et al. (2020). Strain engineering of two-dimensional multilayered heterostructures for beyond-lithium-based rechargeable batteries. *Nat. Comm.* 11, 3297–3297. doi: 10.1038/s41467-020-17014-w
- Yang, L., Liao, H., Tian, Y., Hong, W., and Ji, X. (2019). Rod-Like Sb₂MoO₆: structure evolution and sodium storage for sodium-ion batteries. *Small Methods* 3:1800533. doi: 10.1002/smt.201800533
- Yang, Y., Zhu, H., Xiao, J., Geng, H., Zhang, Y., Zhao, J., et al. (2020). Achieving ultrahigh-rate and high-safety Li⁺ storage based on interconnected tunnel structure in micro-size niobium tungsten oxides. *Adv. Mater.* 32:1905295. doi: 10.1002/adma.201905295
- Yue, Z., Peng, L., Chen, D., and Yu, G. (2016). Intercalation pseudocapacitance in ultrathin VOPO₄ nanosheets: toward high-rate alkali-ion-based electrochemical energy storage. *Nano Lett.* 16, 742–747. doi: 10.1021/acs.nanolett.5b04610
- Zhang, S., Yang, D., Tan, H., Feng, Y., Rui, X., and Yu, Y. (2020). Advances in K-Q (Q = S, Se and SexSy) batteries, mater. *Today*
- Zhang, X., Chen, H., Liu, W., Xiao, N., Zhang, Q., Rui, X., et al. (2020). A long-cycling aqueous zinc-ion pouch cell: NASICON-Type material and surface modification. *Chem. Asian J.* 15, 1430–1435. doi: 10.1002/asia.202000162
- Zhou, K., Zhang, Q., Wang, B., Liu, J., Wen, P., Gui, Z., et al. (2014). The integrated utilization of typical clays in removal of organic dyes and polymer nanocomposites. *J. Clean. Prod.* 81, 281–289. doi: 10.1016/j.jclepro.2014.06.038
- Zhou, K., Zhou, G., and Yuan, H. (2016). Ultrathin 2D VOPO₄ nanosheets: a novel reinforcing agent in polymeric composites. *RSC Adv.* 6, 100344–100351. doi: 10.1039/C6RA24111E
- Zhou, L., Liu, Q., Zhang, Z., Zhang, K., and Mai, L. (2018). Interlayer-spacing-regulated VOPO₄ nanosheets with fast kinetics for high-capacity and durable rechargeable magnesium batteries. *Adv. Mater.* 30:1801984. doi: 10.1002/adma.201801984

Conflict of Interest: The authors declare that the research was conducted in the absence of any commercial or financial relationships that could be construed as a potential conflict of interest.

Copyright © 2020 Zhang, Yang, Liu and Rui. This is an open-access article distributed under the terms of the Creative Commons Attribution License (CC BY). The use, distribution or reproduction in other forums is permitted, provided the original author(s) and the copyright owner(s) are credited and that the original publication in this journal is cited, in accordance with accepted academic practice. No use, distribution or reproduction is permitted which does not comply with these terms.